J. Fluid Mech. (2014), *vol.* 742, *pp* 425–445. © Cambridge University Press 2014
doi:10.1017/jfm.2013.656

Effect of a distant rigid wall on microstreaming generated by an acoustically driven gas bubble

Alexander A. Doinikov† and Ayache Bouakaz

INSERM U930, Université François Rabelais, CHU Bretonneau, 2 Boulevard Tonnellé, 37044 Tours CEDEX 9, France

(Received 17 June 2013; revised 29 October 2013; accepted 9 December 2013; first published online 21 February 2014)

A theory is developed that describes acoustic microstreaming around a gas bubble undergoing small radial and translational oscillations in the presence of a distant rigid wall. It is shown that the presence of the wall can change the amplitude and the phase of the bubble oscillations in such a way that the intensity of acoustic microstreaming is increased considerably as compared with that generated by the same bubble in an infinite liquid. This occurs if the driving frequency is close to the resonance frequency that the bubble has in the presence of the wall. Equations for acoustic microstreaming in the boundary layer at the wall are also provided.

Key words: bubble dynamics, drops and bubbles

1. Introduction

Steady vortical flows that develop around acoustically excited bubbles in a liquid are a well-known phenomenon. In the literature it is referred to as acoustic, or cavitation, microstreaming. Investigations into this phenomenon date back to the 1950s (Kolb & Nyborg 1956; Elder 1959). Conventional practical applications associated with acoustic microstreaming include ultrasonic cleaning of contaminated surfaces, localized micromixing, stimulation of chemical reactions, intensification of heat and mass exchange, etc. Presently interest in this phenomenon is also motivated by the use of microbubble-mediated ultrasound in medicine (see, for example, Goldberg, Raichlen & Forsberg 2001; Khismatullin 2005; Qin, Caskey & Ferrara 2009). It is believed that acoustic microstreaming plays an important role in various biological effects of ultrasound, such as haemolysis, mixing of therapeutic agents in blood, sonothrombolysis and sonoporation. Discussions of these effects can be found in papers by Rooney (1970, 1972), Nyborg (1978), Wu (2002), Marmottant & Hilgenfeldt (2003), Wu & Nyborg (2008) and Collis *et al.* (2010).

Theoretical studies on cavitation microstreaming, making efforts to consider this problem rigourously, are restricted to the case of a bubble in an unbounded liquid. Davidson & Riley (1971) derived equations for microstreaming around a bubble that undergoes translational harmonic oscillations but does not experience radial oscillations. Wu & Du (1997) and Longuet–Higgins (1998) considered the case of a bubble undergoing translational and radial oscillations. Maksimov (2007) extended the result of Longuet–Higgins (1998) so as to include the effect of parametrically

† Email address for correspondence: doinikov@bsu.by

https://doi.org/10.1017/jfm.2013.656 Published online by Cambridge University Press

excited surface modes of high order. Keeping in mind the use of microbubble contrast agents in ultrasound medicine, Liu & Wu (2009) applied the approach of Wu & Du (1997) to calculate microstreaming produced by an encapsulated bubble. Doinikov & Bouakaz (2010*a*,*b*) extended the results of Wu & Du (1997) and Liu & Wu (2009) by taking into account shape oscillations and removing restrictions of the previous derivations, such as the assumption that the thickness of the viscous boundary layer surrounding the bubble is much smaller than the radius of the bubble.

The available theoretical results show that the main contribution to acoustic microstreaming comes from the radial and translational modes of the bubble oscillation. The contribution of surface modes is usually negligible. Exceptions are the case of a large (millimetre-sized) bubble undergoing parametrically excited surface modes of high order in a low-frequency (a few kilohertz) field (Maksimov 2007) and the case of a oscillating liquid drop where the contribution of the surface quadrupole mode may be important (Doinikov & Bouakaz 2010*a*). Such cases are beyond the scope of the present study which mainly aims at applications where micrometre-sized bubbles and high-frequency fields are used.

The purpose of the present paper is to develop a theory that describes acoustic microstreaming that is generated around a gas bubble undergoing small harmonic radial and translational oscillations in the presence of a rigid wall.

2. The first-order field

Consider a gas bubble suspended in a viscous incompressible liquid whose motion is governed by the following equations:

$$\nabla \cdot \boldsymbol{v} = 0, \tag{2.1}$$

$$\rho \frac{\partial \boldsymbol{v}}{\partial t} + \rho(\boldsymbol{v} \cdot \nabla)\boldsymbol{v} = \eta \Delta \boldsymbol{v} - \nabla p, \tag{2.2}$$

where $\boldsymbol{v}$ is the liquid velocity, ρ is the liquid density, η is the dynamic liquid viscosity and p is the liquid pressure. It is assumed that the bubble is situated at a distance d from a rigid wall and undergoes radial and translational oscillations in response to an imposed acoustic pressure field. The motion of the bubble is described in spherical coordinates $(r_1, \theta_1, \varepsilon_1)$ originated at the equilibrium centre of the bubble, as shown in figure 1. It should be noted that the assumption of liquid incompressibility means that the acoustic wavelength is considered to be much larger than all other relevant length scales such as the bubble radius and the distance from the wall d.

The distance d is assumed to be much larger than the viscous penetration depth in the liquid δ_v, which makes it possible to consider separately the viscous liquid motion in the boundary layer at the wall and that in the bulk liquid (around the bubble). Without this assumption, a formidable mathematical problem arises, namely how to find a solution that must satisfy the viscous boundary conditions simultaneously at the bubble surface and at the wall surface and hence have a mathematical form that allows transforming from spherical coordinates at the bubble surface to cylindrical coordinates at the wall. Oguz & Prosperetti (1990) used bispherical coordinates to overcome similar difficulties. Their aim was to calculate the natural frequency of a bubble in the vicinity of a plane free surface. However, they assumed that the bubble underwent linear oscillations and the surrounding liquid was inviscid. It is therefore unclear how their mathematical approach can be generalized, if at all, to the problem of acoustic microstreaming, where viscous and nonlinear solutions are required. The assumption $d \gg \delta_v$ makes the task set in our study amenable to analytical solution.

https://doi.org/10.1017/jfm.2013.656 Published online by Cambridge University Press

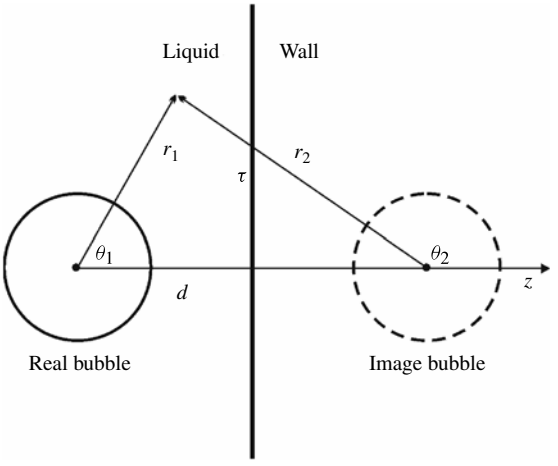


FIGURE 1. Geometry of the problem.

The effect of the wall on the microstreaming around the bubble will be incorporated through a potential solution describing the interaction of the bubble with the wall, which will be obtained by using the method of image sources. The distance d is also assumed to be large compared with the equilibrium bubble radius. It should be mentioned that these assumptions exclude the case of a bubble touching the wall from consideration. This case is of great interest for applications but, as said above, its consideration is hampered by intractable mathematical problems.

2.1. *The first-order field in the bulk liquid*

Linearizing (2.1) and (2.2), one obtains

$$\nabla \cdot \boldsymbol{v}^{(1)} = 0, \tag{2.3}$$

$$\rho \frac{\partial \boldsymbol{v}^{(1)}}{\partial t} = \eta \Delta \boldsymbol{v}^{(1)} - \nabla p^{(1)}, \tag{2.4}$$

where the superscript (1) denotes quantities of first order in the acoustic pressure amplitude. The velocity $\boldsymbol{v}^{(1)}$ can be represented as

$$\boldsymbol{v}^{(1)} = \nabla \varphi + \nabla \times \boldsymbol{\psi}, \tag{2.5}$$

where φ and $\boldsymbol{\psi}$ are the first-order scalar and vorticity velocity potentials. Substituting (2.5) into (2.3) and (2.4) and setting the velocity potential of the incident acoustic wave to be $\varphi_I = A\exp(-\mathrm{i}\omega t)$, one finds that φ and $\boldsymbol{\psi}$ must obey the following equations:

$$\Delta \varphi = 0, \tag{2.6}$$

$$(\Delta + k_v^2)\boldsymbol{\psi} = 0, \tag{2.7}$$

where $k_v = (1 + \mathrm{i})/\delta_v$ is the viscous wavenumber, $\delta_v = \sqrt{2\nu/\omega}$ is the viscous penetration depth and $\nu = \eta/\rho$ is the kinematic liquid viscosity. The scalar potential can be written as

$$\varphi = \varphi_1 + \varphi_2, \tag{2.8}$$

where φ_1 describes the primary scattered wave from the bubble and φ_2 describes a wave that results from the reflection of the primary scattered wave by the wall.

https://doi.org/10.1017/jfm.2013.656 Published online by Cambridge University Press

As the bubble is assumed to execute the radial and translational motions, φ_1 is taken in the following form:

$$\varphi_1 = A\mathrm{e}^{-\mathrm{i}\omega t}\left[\frac{a_1 R_0}{r_1} + b_1\left(\frac{R_0}{r_1}\right)^2 \cos\theta_1\right], \tag{2.9}$$

where R_0 is the equilibrium bubble radius and a_1 and b_1 are constants to be determined by the boundary conditions at the wall and at the bubble surface. According to the method of image sources, the potential of the reflected wave can be written as

$$\varphi_2 = A\mathrm{e}^{-\mathrm{i}\omega t}\left[\frac{a_2 R_0}{r_2} + b_2\left(\frac{R_0}{r_2}\right)^2 \cos\theta_2\right], \tag{2.10}$$

where the coordinates r_2 and θ_2 are introduced as shown in figure 1. The vorticity potential satisfying (2.7) is given by

$$\boldsymbol{\psi} = A\mathrm{e}^{-\mathrm{i}\omega t} c_1 h_1^{(1)}(k_v r_1)\sin\theta_1 \boldsymbol{e}_{\varepsilon 1}, \tag{2.11}$$

where c_1 is a constant, $h_1^{(1)}(x) = -\exp(\mathrm{i}x)(1/x + \mathrm{i}/x^2)$ is the spherical Hankel function of the first kind (Abramowitz & Stegun 1972), and $\boldsymbol{e}_{\varepsilon 1}$ is the unit azimuth vector of the spherical coordinate system related to the bubble. That (2.11) is a solution to (2.7) can be checked by directly substituting (2.11) into (2.7).

In further calculations, expressions for $\nabla\varphi$ and $\nabla\times\psi$ will be used repeatedly so it is helpful to provide them:

$$\nabla\varphi_j = -A\mathrm{e}^{-\mathrm{i}\omega t}\left[\boldsymbol{e}_{rj}\left(\frac{a_j R_0}{r_j^2} + \frac{2b_j R_0^2}{r_j^3}\cos\theta_j\right) + \boldsymbol{e}_{\theta j}\frac{b_j R_0^2}{r_j^3}\sin\theta_j\right], \tag{2.12}$$

$$\nabla\times\boldsymbol{\psi} = A\mathrm{e}^{-\mathrm{i}\omega t}\frac{c_1}{r_1}\left[2\boldsymbol{e}_{r1}h_1^{(1)}(k_v r_1)\cos\theta_1 - \boldsymbol{e}_{\theta 1}\left(h_1^{(1)}(k_v r_1) + k_v r_1 h_1^{(1)\prime}(k_v r_1)\right)\sin\theta_1\right]. \tag{2.13}$$

Here, $j = 1$ or 2 and $h_1^{(1)\prime}(x) = \mathrm{d}h_1^{(1)}(x)/\mathrm{d}x$.

To find relationships between the constants appearing in (2.9) and (2.10), the boundary condition for the normal liquid velocity at the wall is applied:

$$\boldsymbol{n}\cdot\boldsymbol{v}^{(1)} = 0 \quad \text{at } z = d, \tag{2.14}$$

where $\boldsymbol{n} = -\boldsymbol{e}_z$ is the outward normal to the wall. It should be noted that (2.14) results from the assumption that the wall is rigid. In the case of a non-rigid wall, equation (2.14) should be replaced with the conditions of continuity of normal velocities and normal stresses across the liquid–wall interface. To satisfy these conditions, equations describing the behaviour of the wall material should be included in calculations, which complicates finding analytical solutions considerably. Therefore the case of a non-rigid wall is beyond the scope of the present study.

It follows from (2.12) and (2.13) that the contribution of the potential velocity component at the wall is of the order of AR_0/d^2 and that of the rotational velocity component is of the order of $A\exp(-d/\delta_v)/d$. Since $d \gg \delta_v$, the rotational velocity component is negligible as compared with the potential velocity component. Substituting (2.12) into (2.14) and taking into account that at the wall $r_1 = r_2$ and $\theta_2 = \pi - \theta_1$, one finds

$$a_2 = a_1, \quad b_2 = -b_1. \tag{2.15}$$

https://doi.org/10.1017/jfm.2013.656 Published online by Cambridge University Press

To calculate a_1, b_1 and c_1, the boundary conditions at the bubble surface are used. Assuming that there are no impurities and surfactants on the bubble surface and considering that the viscosity of the gas inside the bubble is much smaller than that of the liquid, slippage on the gas–liquid interface can be assumed. A theoretical justification of this assumption can be found in a book by Batchelor (2000). There are also experimental data that confirm the adequacy of this assumption for pulsating bubbles (Crum 1975). It should be noted that the boundary condition of interfacial slippage is not suitable for contrast agent bubbles having a shell. For such bubbles, the boundary condition of adhesion of liquid particles to the bubble shell is more appropriate. To satisfy properly the no-slip condition, the behaviour of the shell material should also be taken into consideration, which makes calculations much more complicated. Therefore this case requires a separate study.

Following the assumption of interfacial slippage, the boundary condition for the tangential liquid velocity is dropped and the boundary condition for the first-order tangential liquid stress $\sigma_{r\theta}$ is taken to be

$$\sigma_{r\theta} = \eta\left(\frac{1}{r_1}\frac{\partial v_{r1}^{(1)}}{\partial \theta_1} + \frac{\partial v_{\theta 1}^{(1)}}{\partial r_1} - \frac{v_{\theta 1}^{(1)}}{r_1}\right) = 0 \quad \text{at } r_1 = R_0, \tag{2.16}$$

where the subscripts $r1$ and $\theta 1$ denote the radial and the tangential components of $\boldsymbol{v}^{(1)}$ in the spherical coordinates related to the bubble. These components are calculated from (2.12) and (2.13), keeping up to terms of second order in the small parameter R_0/d, assuming that a_1 is of zeroth-order and b_1 and c_1 are of second order. As we shall see below, this is true. As a result, (2.16) yields

$$6b_1 = \alpha^2 h_1^{(1)''}(\alpha) c_1, \tag{2.17}$$

with $\alpha = k_v R_0$.

The boundary condition for the normal liquid velocity can be written as

$$\boldsymbol{e}_{r1} \cdot \boldsymbol{v}^{(1)} = \dot{R} + \boldsymbol{e}_{r1} \cdot \boldsymbol{u} \quad \text{at } r_1 = R_0, \tag{2.18}$$

where $R(t)$ is the instantaneous radius of the bubble, $\dot{R} = \mathrm{d}R/\mathrm{d}t$, and $\boldsymbol{u} = u(t)\boldsymbol{e}_z$ is the translational velocity of the bubble. Here $R(t)$ and $u(t)$ can be represented as

$$R(t) = R_0 + \xi_R A \mathrm{e}^{-\mathrm{i}\omega t}, \quad u(t) = \xi_u A \mathrm{e}^{-\mathrm{i}\omega t}. \tag{2.19}$$

Substituting (2.19) along with (2.12) and (2.13) into (2.18) and keeping up to the second order in R_0/d, one obtains

$$a_1 = \mathrm{i}\omega R_0 \xi_R, \quad \xi_u = \frac{a_1 R_0}{4d^2} - \frac{2b_1}{R_0} + \frac{2c_1 h_1^{(1)}(\alpha)}{R_0}. \tag{2.20}$$

Finally, let us apply the boundary condition for the normal stress:

$$P_{g0}\left(\frac{R_0}{R}\right)^{3\gamma} = P_0 - \sigma_{rr} + \frac{2\sigma}{R} \quad \text{at } r_1 = R_0. \tag{2.21}$$

Here, P_{g0} is the equilibrium pressure of the gas inside the bubble, γ is the ratio of specific heats of the gas, P_0 is the hydrostatic pressure in the liquid, σ is the surface tension (assumed to be constant) and σ_{rr} is the radial component of the linear stress tensor of the liquid, given by

$$\sigma_{rr} = -p^{(1)} + 2\eta \frac{\partial v_{r1}^{(1)}}{\partial r_1}, \tag{2.22}$$

https://doi.org/10.1017/jfm.2013.656 Published online by Cambridge University Press

where the linear liquid pressure $p^{(1)}$ can be taken as the following sum:

$$p^{(1)} = p_I + p_S. \tag{2.23}$$

The quantity p_I denotes the incident wave pressure, given by

$$p_I = -\rho \frac{\partial \varphi_I}{\partial t} = \mathrm{i}\omega\rho A \mathrm{e}^{-\mathrm{i}\omega t}, \tag{2.24}$$

and p_S is the scattered pressure. Substituting (2.5) into (2.4) and using (2.6), (2.7) and the condition that $p_S \to 0$ as $r_1 \to \infty$, one can show that

$$p_S = -\rho \frac{\partial \varphi}{\partial t}. \tag{2.25}$$

Using (2.8)–(2.10) to calculate φ accurate up to the second order in R_0/d, (2.12) and (2.13) to calculate $\partial v_{r1}^{(1)}/\partial r_1$ with the same accuracy, substituting then (2.22)–(2.25) into (2.21), and using (2.19) for R, one obtains

$$a_1 = \left(\frac{\omega_0^2}{\omega^2} - 1 - \frac{R_0}{2d} - \mathrm{i}\delta \right)^{-1}, \tag{2.26}$$

where ω_0 is the angular resonance frequency of the bubble in an infinite liquid, given by

$$\omega_0 = \frac{1}{R_0} \left(\frac{3\gamma P_0}{\rho} + \frac{2(3\gamma - 1)\sigma}{\rho R_0} \right)^{1/2}, \tag{2.27}$$

and δ is the viscous damping constant, defined as

$$\delta = \frac{4\nu}{\omega R_0^2}. \tag{2.28}$$

Recall that we assume the liquid to be incompressible and non-heat-conducting, which results in the neglect of radiation and thermal damping. However, if necessary, these types of damping can be taken into account via (2.28) using a method suggested by Prosperetti (1974, 1977), namely, treating ν in (2.28) as an effective viscosity and suitably increasing its value.

Equation (2.21) also gives

$$c_1 = a_1 \left(\frac{R_0}{2d} \right)^2 \frac{6\alpha^2 \exp(-\mathrm{i}\alpha)}{18\mathrm{i} + 18\alpha - 3\mathrm{i}\alpha^2 - \alpha^3}, \tag{2.29}$$

if (2.17) is taken into account. Finally, substitution of (2.29) into (2.17) and (2.20) yields

$$b_1 = a_1 \left(\frac{R_0}{2d} \right)^2 \frac{\alpha^3 + 3\mathrm{i}\alpha^2 - 6\alpha - 6\mathrm{i}}{18\mathrm{i} + 18\alpha - 3\mathrm{i}\alpha^2 - \alpha^3}, \tag{2.30}$$

$$\xi_u = a_1 \frac{3R_0}{4d^2} \frac{6\mathrm{i} + 6\alpha - 3\mathrm{i}\alpha^2 - \alpha^3}{18\mathrm{i} + 18\alpha - 3\mathrm{i}\alpha^2 - \alpha^3}. \tag{2.31}$$

2.2. *The first-order field in the boundary layer at the wall*

An approach that allows one to evaluate the sound field in the boundary layer at the wall is described by Landau & Lifshitz (1987). As is shown in § 24 of their book, if $\delta_v \ll d$, the expression for the normal velocity component can be taken as if the

https://doi.org/10.1017/jfm.2013.656 Published online by Cambridge University Press

liquid flow were potential, i.e. from (2.8) to (2.10), and the variation of the tangential velocity component within the boundary layer can be represented as

$$v_\tau^{(1)} = v_{\tau 0}^{(1)}\{1 - \exp[\mathrm{i}k_v(d-z)]\}, \tag{2.32}$$

where $v_{\tau 0}^{(1)}$ is the value of the tangential velocity component at the wall ($z = d$) which corresponds to the potential liquid flow. It follows from (2.8) to (2.10) that

$$v_{\tau 0}^{(1)} = -A\mathrm{e}^{-\mathrm{i}\omega t}\left[\frac{2a_1R_0\tau}{(d^2+\tau^2)^{3/2}} + \frac{6b_1R_0^2\tau\,\mathrm{d}}{(d^2+\tau^2)^{5/2}}\right], \tag{2.33}$$

where $\tau = \sqrt{x^2+y^2}$ is the distance from the axis z along the wall surface.

3. Acoustic streaming

3.1. *Acoustic streaming in the bulk liquid*

By averaging (2.1) and (2.2) over time and keeping up to the second order in the acoustic pressure amplitude, one obtains the equations of acoustic streaming:

$$\nabla \cdot \boldsymbol{V} = 0, \tag{3.1}$$

$$\eta\Delta\boldsymbol{V} - \nabla P = \rho\langle(\boldsymbol{v}^{(1)}\cdot\nabla)\boldsymbol{v}^{(1)}\rangle, \tag{3.2}$$

where $\langle\rangle$ means the time average and $\boldsymbol{V}$ and P are the velocity and the pressure fields of acoustic streaming. To satisfy (3.1), $\boldsymbol{V}$ is taken as

$$\boldsymbol{V} = \nabla\times\boldsymbol{\Psi}. \tag{3.3}$$

Substituting (3.3) into (3.2) and applying the curl operator, one has

$$\Delta^2\boldsymbol{\Psi} = -\frac{1}{\nu}\nabla\times\langle(\boldsymbol{v}^{(1)}\cdot\nabla)\boldsymbol{v}^{(1)}\rangle. \tag{3.4}$$

Substituting (2.5), making use of (2.7), and keeping up to the second-order in R_0/d, one gets

$$\Delta^2\boldsymbol{\Psi} = -\frac{1}{\nu}\nabla\times\langle k_v^2\boldsymbol{\psi}\times\nabla\varphi_1\rangle = -\frac{1}{2\nu}\mathrm{Re}\{\nabla\times(k_v^2\boldsymbol{\psi}\times\nabla\varphi_1^*)\}, \tag{3.5}$$

where Re means 'the real part of' and the asterisk indicates the complex conjugate. Finally, substituting (2.11) and (2.12) and using the explicit expression for $h_1^{(1)}$, one finds

$$\Delta^2\boldsymbol{\Psi} = \frac{|A|^2R_0}{2\nu}\frac{\sin\theta_1}{r_1^5}\boldsymbol{e}_{\varepsilon 1}\mathrm{Re}\{\mathrm{i}a_1^*c_1\exp(\mathrm{i}k_vr_1)(3-3\mathrm{i}k_vr_1-k_v^2r_1^2)\}. \tag{3.6}$$

Equation (3.6) suggests that $\boldsymbol{\Psi}$ can be sought in the following form:

$$\boldsymbol{\Psi} = \frac{|A|^2R_0}{2\nu}\sin\theta_1\boldsymbol{e}_{\varepsilon 1}\mathrm{Re}\{\mathrm{i}a_1^*c_1G(r_1)\}. \tag{3.7}$$

Substitution of (3.7) into (3.6) gives

$$G^{\mathrm{IV}} + \frac{4}{r_1}G''' - \frac{4}{r_1^2}G'' = \frac{1}{r_1^5}\exp(\mathrm{i}k_vr_1)(3-3\mathrm{i}k_vr_1-k_v^2r_1^2). \tag{3.8}$$

A solution to this equation can be found by the method of variation of parameters, also known as the Lagrange method. This is a general method to solve inhomogeneous

https://doi.org/10.1017/jfm.2013.656 Published online by Cambridge University Press

linear ordinary differential equations; see, for example, § 4.4 in the book by Boyce & DiPrima (2001). As a result, the function $G(r_1)$ is found to be

$$G(r_1) = A_1(r_1)r_1^{-2} + A_2(r_1) + A_3(r_1)r_1 + A_4(r_1)r_1^3, \tag{3.9}$$

where the functions $A_n(r_1)$ are given by

$$A_1(r_1) = B_1 - \frac{1}{30\mathrm{i}k_v}\exp(\mathrm{i}k_v r_1)(8 - 5\mathrm{i}k_v r_1 - k_v^2 r_1^2), \tag{3.10}$$

$$A_2(r_1) = B_2 + \frac{\mathrm{i}k_v}{6}\exp(\mathrm{i}k_v r_1) + \frac{1}{2}\int_{R_0}^{r_1} s^{-2}\exp(\mathrm{i}k_v s)(1 - \mathrm{i}k_v s)\,\mathrm{d}s, \tag{3.11}$$

$$A_3(r_1) = B_3 - \frac{1}{6}\int_{R_0}^{r_1} s^{-3}\exp(\mathrm{i}k_v s)(3 - 3\mathrm{i}k_v s - k_v^2 s^2)\,\mathrm{d}s, \tag{3.12}$$

$$A_4(r_1) = B_4 + \frac{1}{30}\int_{R_0}^{r_1} s^{-5}\exp(\mathrm{i}k_v s)(3 - 3\mathrm{i}k_v s - k_v^2 s^2)\,\mathrm{d}s. \tag{3.13}$$

The quantities B_n are constants to be determined by the boundary conditions at infinity and at the bubble surface. From the condition that $\boldsymbol{V} \to 0$ as $r_1 \to \infty$, one obtains

$$B_3 = \frac{1}{6}\int_{R_0}^{\infty} s^{-3}\exp(\mathrm{i}k_v s)(3 - 3\mathrm{i}k_v s - k_v^2 s^2)\,\mathrm{d}s, \tag{3.14}$$

$$B_4 = -\frac{1}{30}\int_{R_0}^{\infty} s^{-5}\exp(\mathrm{i}k_v s)(3 - 3\mathrm{i}k_v s - k_v^2 s^2)\,\mathrm{d}s. \tag{3.15}$$

To find the boundary conditions for the acoustic streaming at the bubble surface, the following approach is employed. The tangential stress and the normal velocity are calculated at the perturbed surface of the bubble which is described by the following equation:

$$\boldsymbol{r}_s = z_c(t)\boldsymbol{e}_z + R(t)\boldsymbol{e}_{r1}, \tag{3.16}$$

where $\boldsymbol{r}_s$ is the position vector of the surface points, $z_c(t)$ is the displacement of the bubble centre along the axis z, defined as $\dot{z}_c(t) = u(t)$, and $R(t)$ and $u(t)$ are given by (2.19). The calculation is carried with accuracy up to the second-order in the acoustic pressure amplitude and then averaging over time is performed. As a result, the boundary condition for the tangential stress takes the form

$$T_{r\theta} + \langle A\mathrm{e}^{-\mathrm{i}\omega t}[(\mathrm{i}\xi_u/\omega)\boldsymbol{e}_z + \xi_R\boldsymbol{e}_{r1}]\cdot\nabla\sigma_{r\theta}\rangle = 0 \quad \text{at } r_1 = R_0, \tag{3.17}$$

where $T_{r\theta}$ denotes the tangential stress generated by the acoustic streaming, defined as

$$T_{r\theta} = \eta\left(\frac{1}{r_1}\frac{\partial V_{r1}}{\partial\theta_1} + \frac{\partial V_{\theta 1}}{\partial r_1} - \frac{V_{\theta 1}}{r_1}\right), \tag{3.18}$$

where V_{r1} and $V_{\theta 1}$ are the radial and tangential components of $\boldsymbol{V}$. Substitution of (3.7) into (3.3) yields

$$\boldsymbol{V} = \frac{|A|^2 R_0}{\nu}\left[\boldsymbol{e}_{r1}\frac{\cos\theta_1}{r_1}\mathrm{Re}\{ia_1^* c_1 G(r_1)\} - \boldsymbol{e}_{\theta 1}\frac{\sin\theta_1}{2r_1}\mathrm{Re}\{\mathrm{i}a_1^* c_1(G(r_1) + r_1 G'(r_1))\}\right]. \tag{3.19}$$

Upon substitution of (3.19) into (3.18), one obtains

$$T_{r\theta} = -\tfrac{1}{2}\rho|A|^2 R_0\sin\theta_1\mathrm{Re}\{\mathrm{i}a_1^* c_1 G''(r_1)\}. \tag{3.20}$$

https://doi.org/10.1017/jfm.2013.656 Published online by Cambridge University Press

Substituting (3.20) along with all of the necessary equations from § 2.1 into (3.17) and keeping up to the second order in R_0/d, one has

$$G''(R_0) = \frac{\exp(\mathrm{i}\alpha)}{R_0^3}. \tag{3.21}$$

Finally, calculating $G^{\mathrm{II}}(R_0)$ from (3.9) and substituting into (3.21), one finds B_1 to be

$$B_1 = \frac{\mathrm{i}(\alpha^2 - 8)}{30k_v}\exp(\mathrm{i}\alpha) - R_0^5 B_4. \tag{3.22}$$

Let us now apply the boundary condition for the normal velocity. By analogy with (3.17), one can write

$$V_{r1} + \boldsymbol{e}_{r1}\cdot\langle A\mathrm{e}^{-\mathrm{i}\omega t}\{[(\mathrm{i}\xi_u/\omega)\boldsymbol{e}_z + \xi_R\boldsymbol{e}_{r1}]\cdot\nabla\}\boldsymbol{v}^{(1)}\rangle = 0 \quad \text{at } r_1 = R_0. \tag{3.23}$$

This condition assumes that the bubble can be considered as immobile with respect to the acoustic streaming generated by its linear oscillations. It should be noted that in reality the bubble will drift due to acoustic radiation forces; however, the contribution of this effect into acoustic streaming is of the second order of smallness as compared with that of the linear oscillatory motion. Calculating V_{r1} from (3.19) and substituting it along with the linear solutions into (3.23), one finds, with accuracy up to $(R_0/d)^2$,

$$G(R_0) = \frac{3 + \mathrm{i}\alpha}{6\alpha^2 R_0}\exp(\mathrm{i}\alpha), \tag{3.24}$$

whence it follows that

$$B_2 = \frac{3 + \mathrm{i}\alpha - \alpha^2 - \mathrm{i}\alpha^3}{6\alpha^2 R_0}\exp(\mathrm{i}\alpha) - R_0 B_3. \tag{3.25}$$

Now that all of the quantities appearing in (3.9) are known, it is useful to calculate also explicit expressions for the derivatives $G'(r_1)$ and $G''(r_1)$ appearing in (3.19) and (3.20). The result is

$$G'(r_1) = -2r_1^{-3}A_1(r_1) + A_3(r_1) + 3r_1^2 A_4(r_1), \tag{3.26}$$

$$G''(r_1) = 6r_1^{-4}A_1(r_1) + 6r_1 A_4(r_1). \tag{3.27}$$

We now proceed to the calculation of the time-averaged radial component of the stress tensor which is defined as

$$T_{rr} = -P + 2\eta\frac{\partial V_{r1}}{\partial r_1}. \tag{3.28}$$

To find P, (3.2) is reworked, with accuracy up to $(R_0/d)^2$, as follows:

$$\begin{aligned}
\nabla P &= \eta\Delta\boldsymbol{V} - \rho\langle(\boldsymbol{v}^{(1)}\cdot\nabla)\boldsymbol{v}^{(1)}\rangle = \eta\Delta\boldsymbol{V} - \rho\langle\tfrac{1}{2}\nabla(\boldsymbol{v}^{(1)}\cdot\boldsymbol{v}^{(1)}) - \boldsymbol{v}^{(1)}\times(\nabla\times\boldsymbol{v}^{(1)})\rangle \\
&= \eta\Delta\boldsymbol{V} - \rho\langle\tfrac{1}{2}\nabla(\boldsymbol{v}^{(1)}\cdot\boldsymbol{v}^{(1)}) + \boldsymbol{v}^{(1)}\times(\Delta\boldsymbol{\psi})\rangle \\
&= \eta\Delta\boldsymbol{V} - \rho\langle\tfrac{1}{2}\nabla(\boldsymbol{v}^{(1)}\cdot\boldsymbol{v}^{(1)}) + k_v^2\boldsymbol{\psi}\times\nabla\varphi_1\rangle \\
&= -\eta\nabla\times(\nabla\times\boldsymbol{V}) - \tfrac{1}{2}\rho\mathrm{Re}\{k_v^2\boldsymbol{\psi}\times\nabla\varphi_1^*\} - \tfrac{1}{4}\rho\nabla(\boldsymbol{v}^{(1)}\cdot\boldsymbol{v}^{(1)*}).
\end{aligned} \tag{3.29}$$

https://doi.org/10.1017/jfm.2013.656 Published online by Cambridge University Press

Substitution of (3.19), (2.11) and (2.12) into the first two terms of (3.29) yields

$$\begin{aligned}\nabla P = {} & \rho R_0|A|^2\left[\boldsymbol{e}_{r1}\cos\theta_1\mathrm{Re}\left\{\mathrm{i}a_1^*c_1\left(10A_4-\frac{2A_2}{r_1^3}\right)\right\}\right.\\ & \left.-\boldsymbol{e}_{\theta1}\frac{\sin\theta_1}{r_1}\mathrm{Re}\left\{ia_1^*c_1\left(10r_1A_4+\frac{A_2}{r_1^2}+\frac{1-\mathrm{i}k_vr_1}{2r_1^3}\exp(\mathrm{i}k_vr_1)\right)\right\}\right]\\ & -\frac{1}{4}\rho\nabla(\boldsymbol{v}^{(1)}\cdot\boldsymbol{v}^{(1)*}).\end{aligned} \tag{3.30}$$

It is easy to check, using (3.11) and (3.13), that the first term on the right-hand side of (3.30) is the gradient of the following function:

$$S=\rho R_0|A|^2\cos\theta_1\mathrm{Re}\left\{\mathrm{i}a_1^*c_1\left(10r_1A_4+\frac{A_2}{r_1^2}+\frac{1-\mathrm{i}k_vr_1}{2r_1^3}\exp(\mathrm{i}k_vr_1)\right)\right\}. \tag{3.31}$$

Therefore P can be written as

$$P=S-\tfrac{1}{4}\rho\nabla(\boldsymbol{v}^{(1)}\cdot\boldsymbol{v}^{(1)*}). \tag{3.32}$$

On substitution of the linear solutions into the second term on the right-hand side of (3.32), one finds

$$\begin{aligned}P = {} & \frac{\rho|A|^2}{r_1^2}\left[\frac{|a_1|^2}{4}\left(\frac{R_0^2\cos\theta_1}{2d^2}-\frac{R_0^2}{r_1^2}\right)+\frac{R_0\cos\theta_1}{r_1}\right.\\ & \left.\times\ \mathrm{Re}\left\{\mathrm{i}a_1^*c_1\left(10r_1^4A_4+r_1A_2+\frac{(1-\mathrm{i}k_vr_1)(k_v^2r_1^2-2)\exp(\mathrm{i}k_vr_1)}{2k_v^2r_1^2}\right)-a_1^*b_1\frac{R_0^2}{r_1^2}\right\}\right].\end{aligned} \tag{3.33}$$

Finally, using (3.19), one finds the part of T_{rr} which is caused by viscous stresses to be

$$T_{rr}^{(vis)}=2\eta\frac{\partial V_{r1}}{\partial r_1}=\frac{\rho|A|^2R_0\cos\theta_1}{r_1^4}\mathrm{Re}\{\mathrm{i}a_1^*c_1(4r_1^5A_4-2r_1^2A_2-6A_1)\}. \tag{3.34}$$

To sum up, the main results of this subsection are given by (3.19) and (3.20). These equations describe the velocity field and the tangential stress of the acoustic microstreaming which is generated around the bubble in the presence of the wall. The function $G(r_1)$ and its derivatives which appear in these equations are given by (3.9), (3.26) and (3.27).

3.2. *Lagrangian streaming velocity*

For comparison with experiments it is important to know the Lagrangian streaming velocity which is defined as

$$\boldsymbol{V}_L=\boldsymbol{V}+\boldsymbol{V}_S, \tag{3.35}$$

where $\boldsymbol{V}$ is given by (3.19) and $\boldsymbol{V}_S$, known as the Stokes drift velocity, is calculated by

$$\boldsymbol{V}_S=\left\langle\int\boldsymbol{v}^{(1)}\,\mathrm{d}t\cdot\nabla\boldsymbol{v}^{(1)}\right\rangle, \tag{3.36}$$

see, for example, (Longuet–Higgins 1998). Equation (3.36) can be transformed into

$$\boldsymbol{V}_S=\frac{1}{2\omega}\mathrm{Re}\{\mathrm{i}(\boldsymbol{v}^{(1)}\cdot\nabla)\boldsymbol{v}^{(1)*}\}. \tag{3.37}$$

https://doi.org/10.1017/jfm.2013.656 Published online by Cambridge University Press

On substitution of (2.5), (2.12) and (2.13), with accuracy up to $(R_0/d)^2$, one finds the radial and tangential components of $\boldsymbol{V}_S$ to be

$$V_{Sr} = \frac{|A|^2 R_0^3 \cos\theta_1}{6\omega\ r_1^6}\mathrm{Re}\left\{\mathrm{i}a_1^* c_1\left[\frac{\exp(\mathrm{i}\alpha)}{\alpha^2}(\alpha^3+3\mathrm{i}\alpha^2-6\alpha-6\mathrm{i})\right.\right.$$
$$\left.\left.+\ \frac{6\exp(\mathrm{i}k_v r_1)}{\alpha^2}(\mathrm{i}+k_v r_1-\mathrm{i}k_v^2 r_1^2)\right]\right\}, \tag{3.38}$$

$$V_{S\theta} = \frac{|A|^2 R_0^3 \sin\theta_1}{3\omega r_1^6}\mathrm{Re}\left\{\mathrm{i}a_1^* c_1\left[\frac{\exp(\mathrm{i}\alpha)}{\alpha^2}(\alpha^3+3\mathrm{i}\alpha^2-6\alpha-6\mathrm{i})\right.\right.$$
$$\left.\left.+\ \frac{3\exp(\mathrm{i}k_v r_1)}{2\alpha^2}(4\mathrm{i}+4k_v r_1-3\mathrm{i}k_v^2 r_1^2-k_v^3 r_1^3)\right]\right\}. \tag{3.39}$$

3.3. *Acoustic streaming in the boundary layer at the wall*

Let us now apply (3.2) to the boundary layer at the wall. The derivation presented in this subsection is based on assumptions commonly used in the boundary-layer theory. A detailed discussion of these assumptions can be found in many books on hydrodynamics; see, for example, books by Lamb (1975), Schlichting (1979) or Batchelor (2000). The boundary-layer theory assumes that viscous effects are important only within a thin boundary layer and outside this layer the fluid motion occurs as if that were an inviscid fluid. The boundary-layer thickness is supposed to be small compared with distances parallel to the boundary over which the flow velocity changes appreciably. It follows from these assumptions that, first, the normal velocity component within the boundary layer can be taken to be zero and hence the streaming velocity has only a tangential component. Second, the derivative with respect to z in $\Delta\boldsymbol{V}$ is much larger than those with respect to the coordinates parallel to the wall. With these assumptions, (3.2) is reduced to

$$\eta\frac{\partial^2 V_\tau}{\partial z^2}-\frac{\partial P}{\partial\tau}=\rho\left\langle v_\tau^{(1)}\frac{\partial v_\tau^{(1)}}{\partial\tau}\right\rangle=\frac{\rho}{2}\frac{\partial}{\partial\tau}\langle(v_\tau^{(1)})^2\rangle=\frac{\rho}{4}\frac{\partial}{\partial\tau}(v_\tau^{(1)}v_\tau^{(1)*}), \tag{3.40}$$

where V_τ denotes the tangential velocity component within the boundary layer. Substitution of (2.32) into (3.40) yields

$$\eta\frac{\partial^2 V_\tau}{\partial z^2}-\frac{\partial P}{\partial\tau} = \frac{\rho}{4}\frac{\partial}{\partial\tau}(v_{\tau0}^{(1)}v_{\tau0}^{(1)*})+\frac{\rho}{4}\frac{\partial}{\partial\tau}(v_{\tau0}^{(1)}v_{\tau0}^{(1)*})\{\exp[2(z-d)/\delta_v]$$
$$-2\exp[(z-d)/\delta_v]\cos[(z-d)/\delta_v]\}. \tag{3.41}$$

This equation can be divided into two equations (Nyborg 1958):

$$\frac{\partial P}{\partial\tau}=-\frac{\rho}{4}\frac{\partial}{\partial\tau}(v_{\tau0}^{(1)}v_{\tau0}^{(1)*}) \tag{3.42}$$

and

$$\eta\frac{\partial^2 V_\tau}{\partial z^2}=\frac{\rho}{4}\frac{\partial}{\partial\tau}(v_{\tau0}^{(1)}v_{\tau0}^{(1)*})\{\exp[2(z-d)/\delta_v]-2\exp[(z-d)/\delta_v]\cos[(z-d)/\delta_v]\}. \tag{3.43}$$

Equation (3.42) gives the time-averaged pressure in the wall boundary layer:

$$P=-\frac{\rho}{4}(v_{\tau0}^{(1)}v_{\tau0}^{(1)*}). \tag{3.44}$$

https://doi.org/10.1017/jfm.2013.656 Published online by Cambridge University Press

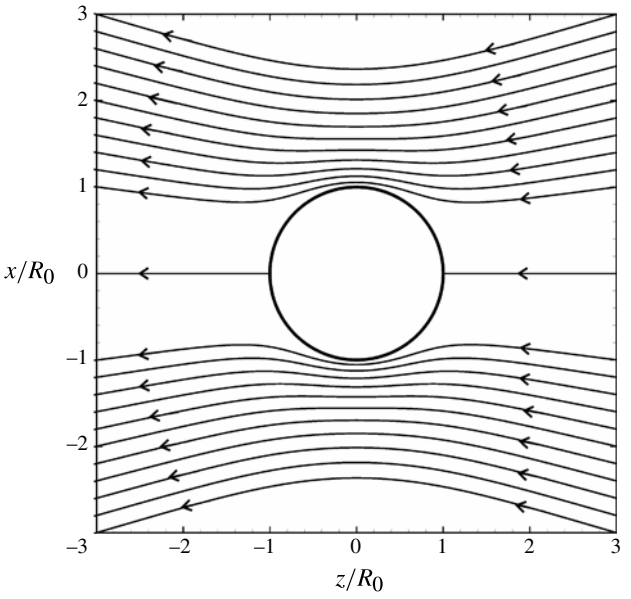


FIGURE 2. Example of streamlines given by (3.19). Calculations were made at $R_0 = 5$ μm and $d = 5R_0$.

Integrating (3.43) and taking into account that $V_\tau = 0$ at $z = d$ and that V_τ must be finite at $d - z \to \infty$, one obtains

$$V_\tau = \frac{1}{2\omega}\frac{\partial}{\partial \tau}(v_{\tau 0}^{(1)} v_{\tau 0}^{(1)*}) \left\{ \frac{1}{4}\exp[2(z-d)/\delta_v] - \exp[(z-d)/\delta_v]\sin[(z-d)/\delta_v] - \frac{1}{4} \right\}. \tag{3.45}$$

The tangential stress exerted on the wall surface is calculated as

$$T_\tau = -\eta \left(\frac{\partial V_\tau}{\partial z} \right)_{z=d} = \frac{\rho \delta_v}{8}\frac{\partial}{\partial \tau}(v_{\tau 0}^{(1)} v_{\tau 0}^{(1)*}). \tag{3.46}$$

If there is an object near the wall whose size is much smaller than the thickness of the boundary layer at the wall, the shear stress experienced by this object should be of the same order as that given by (3.46). Equation (3.45) and (3.46) are in agreement with the results of Nyborg (1958); see (19) and (22) in his paper.

4. Numerical examples

The values of the physical parameters used in our simulations are as follows: $P_0 = 101.3$ kPa, $\rho = 1000$ kg m^{-3}, $\eta = 0.001$ Pa s, $\sigma = 0.072$ N m^{-1}, $\gamma = 1.4$, and the speed of sound in the liquid $c = 1500$ m s^{-1}. These values correspond to an air bubble in water. Figure 2 shows streamlines of the acoustic microstreaming around the bubble. The wall is supposed to be at the right. The streamlines were calculated by (3.19). All spatial sizes are scaled by R_0. The pattern of the streamlines is similar to that obtained by Longuet–Higgins (1998) for a bubble in an infinite liquid. This is not surprising since we assume that the wall is situated far from the bubble. However, the presence of the wall can increase considerably the intensity of the streaming. To demonstrate this effect, we make a comparison with the theory developed by

https://doi.org/10.1017/jfm.2013.656 Published online by Cambridge University Press

Longuet–Higgins (1998) for a bubble in an infinite liquid. From (8.27) in his work it follows that the radial and tangential velocities of the microstreaming arising around a bubble in an infinite liquid can be calculated as

$$V_{rLH} = -\frac{a_R a_T}{R_0}\left[\sin\phi\left(\frac{R_0}{r_1}+\frac{R_0^3}{2r_1^3}\right)+\frac{3\delta_v}{R_0}(\cos\phi+\sin\phi)\left(\frac{R_0}{r_1}-\frac{R_0^3}{r_1^3}\right)\right]\cos\theta_1, \quad (4.1)$$

$$V_{\theta LH} = \frac{a_R a_T}{2R_0}\left[\sin\phi\left(\frac{R_0}{r_1}-\frac{R_0^3}{2r_1^3}\right)+\frac{3\delta_v}{R_0}(\cos\phi+\sin\phi)\left(\frac{R_0}{r_1}+\frac{R_0^3}{r_1^3}\right)\right]\sin\theta_1, \quad (4.2)$$

where a_R is the amplitude of the bubble radial oscillation, a_T is the amplitude of the bubble translational velocity and ϕ is the phase difference between the radial oscillation and the translational velocity. Substituting (4.1) and (4.2) into (3.18), one finds the tangential stress to be

$$T_{r\theta LH} = \frac{3\eta R_0^2 a_R a_T}{2r_1^4}\left[\sin\phi-\frac{6\delta_v}{R_0}(\cos\phi+\sin\phi)\right]\sin\theta_1. \quad (4.3)$$

Let us assume that the bubble is set in motion by a plane travelling wave with the velocity potential $\varphi_I = A\exp(\mathrm{i}kz-\mathrm{i}\omega t)$, where $k=\omega/c$ is the wave vector. In this case, a_R is given by

$$a_R = A\left(\omega R_0\sqrt{(\omega_0^2/\omega^2-1)^2+\delta^2}\right)^{-1}. \quad (4.4)$$

The translational velocity of the bubble can be taken to be equal to $3\boldsymbol{v}_I$, where $\boldsymbol{v}_I = \boldsymbol{\nabla}\varphi_I$; see, for example, Landau & Lifshitz (1987, p. 31). It follows that a_T equals

$$a_T = 3\omega A/c, \quad (4.5)$$

and ϕ is given by

$$\phi = \pi+\arctan[\delta/(1-\omega_0^2/\omega^2)]. \quad (4.6)$$

These equations were used to calculate the dashed curves in figure 3 which show the amplitudes of the radial velocity, the tangential velocity and the tangential stress in an infinite liquid as a function of the driving frequency ω. The amplitudes were calculated for a bubble with $R_0=5$ μm at $r_1=R_0+2\delta_v$, i.e. at the distance $2\delta_v$ from the equilibrium surface of the bubble. The solid curves show analogous quantities for the same bubble in the presence of a wall at $d=5R_0$. They were calculated by (3.19) and (3.20). It should be emphasized that these curves were calculated assuming that the translational motion of the bubble is caused by the wave scattered by the bubble and reflected from the wall, the contribution of the primary incident wave being left out. The velocity amplitudes are normalized by $A^2/(cR_0^2)$ and the stress amplitude is normalized by $\eta A^2/(cR_0^3)$. The choice of these normalization factors is based on the expressions for a_R and a_T; see (4.4) and (4.5). The peaks on the solid curves correspond to the bubble resonance frequency in the presence of the wall. From (2.26) it follows that this frequency is given by

$$\omega_{0w} = \omega_0(1+R_0/2d)^{-1/2}. \quad (4.7)$$

In the case shown in figure 3, $\omega_{0w}/\omega_0=0.953$. Figure 3 demonstrates that if the bubble is driven near ω_{0w}, the intensity of microstreaming in the presence of the wall is much greater than that in an infinite liquid.

Figure 4 shows the ratios $|V_r/V_{rLH}|$, $|V_\theta/V_{\theta LH}|$ and $|T_{r\theta}/T_{r\theta LH}|$ as a function of d for a bubble with $R_0=5$ μm at $r_1=R_0+2\delta_v$ and $\omega=\omega_{0w}$. Figure 5 shows the dependence

https://doi.org/10.1017/jfm.2013.656 Published online by Cambridge University Press

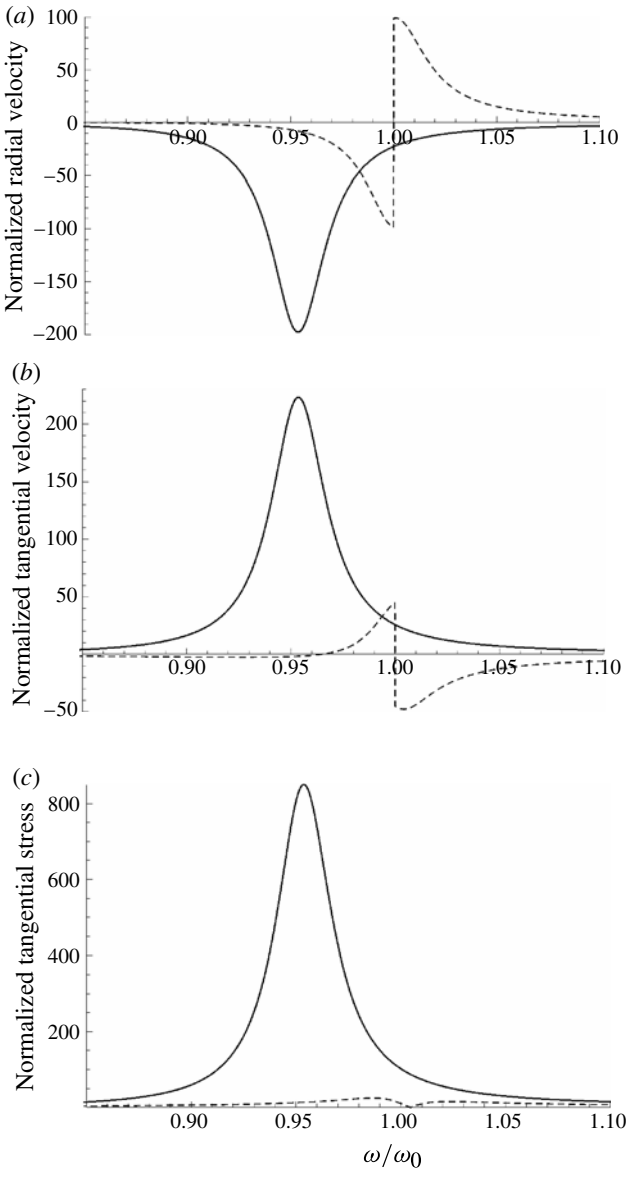


FIGURE 3. Comparison of streaming flows that are generated around a bubble in an infinite liquid and in the presence of a wall at different values of the driving frequency ω. The dashed lines correspond to a bubble in an infinite liquid and the solid lines show the streaming characteristics for the same bubble in the presence of a wall. Calculations were made at $R_0 = 5$ μm, $r_1 = R_0 + 2\delta_v$ and $d = 5R_0$.

of the same ratios on R_0 at $d = 5R_0$, $r_1 = R_0 + 2\delta_v$ and $\omega = \omega_{0w}$. The values of V_r, V_θ and $T_{r\theta}$ were calculated by (3.19) and (3.20), and those of V_{rLH}, $V_{\theta LH}$ and $T_{r\theta LH}$ by (4.1)–(4.6). The peaks in figures 4(*b*) and 5(*b*) are explained by the fact that $V_{\theta LH}$ goes through zero in the range being considered as seen in figure 3(*b*), therefore for certain parameters the ratio $|V_\theta / V_{\theta LH}|$ can tend to infinity. Figures 4 and 5 demonstrate that the effect of the wall on acoustic microstreaming increases with decreasing d

https://doi.org/10.1017/jfm.2013.656 Published online by Cambridge University Press

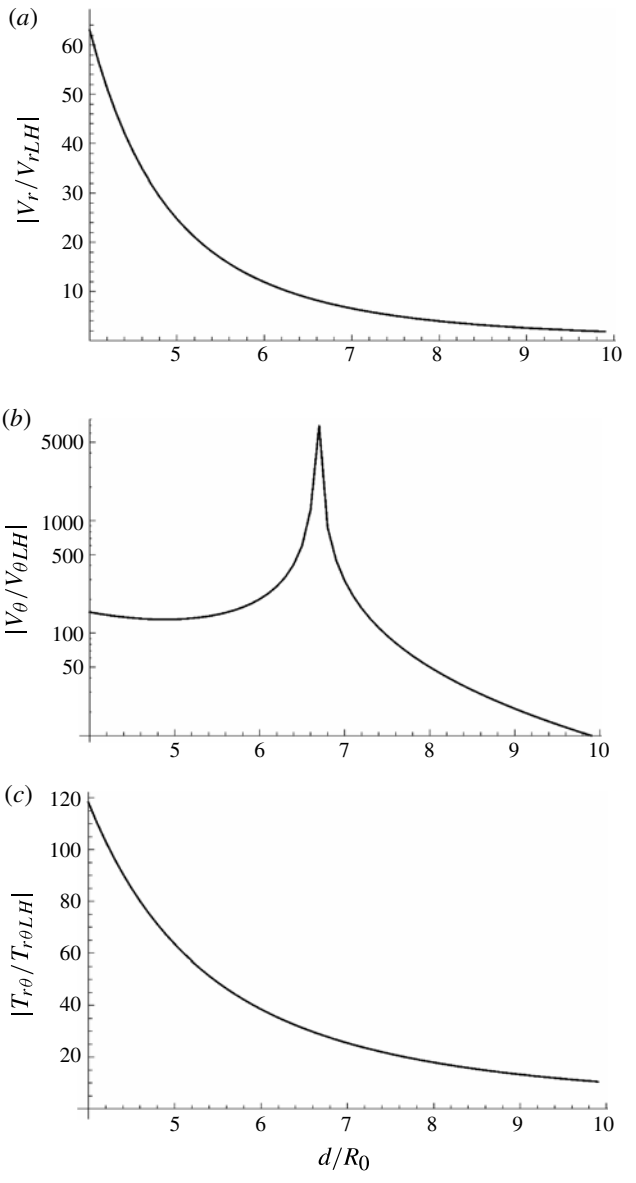


FIGURE 4. Comparison of the streaming characteristics for a bubble in an infinite liquid and in the presence of a wall at different values of d. Calculations were made at $R_0 = 5$ μm, $r_1 = R_0 + \delta_v$ and $\omega = \omega_{0w}$.

and increasing R_0. This result is easily explicable. A reduction in d or an increase in R_0 increase the intensity of the reflected wave and hence the intensity of the bubble oscillations.

Figures 6 and 7 allow one to understand why the presence of a wall increases the intensity of acoustic microstreaming. Figure 6(*a*) shows the ratio of the amplitude of the bubble radial oscillation in the presence of the wall, $|A\xi_R|$, to that in an infinite liquid, a_R, as a function of the driving frequency for a bubble with $R_0 = 5$ μm at $d = 5R_0$. The radial oscillation amplitude in the presence of the wall is calculated

https://doi.org/10.1017/jfm.2013.656 Published online by Cambridge University Press

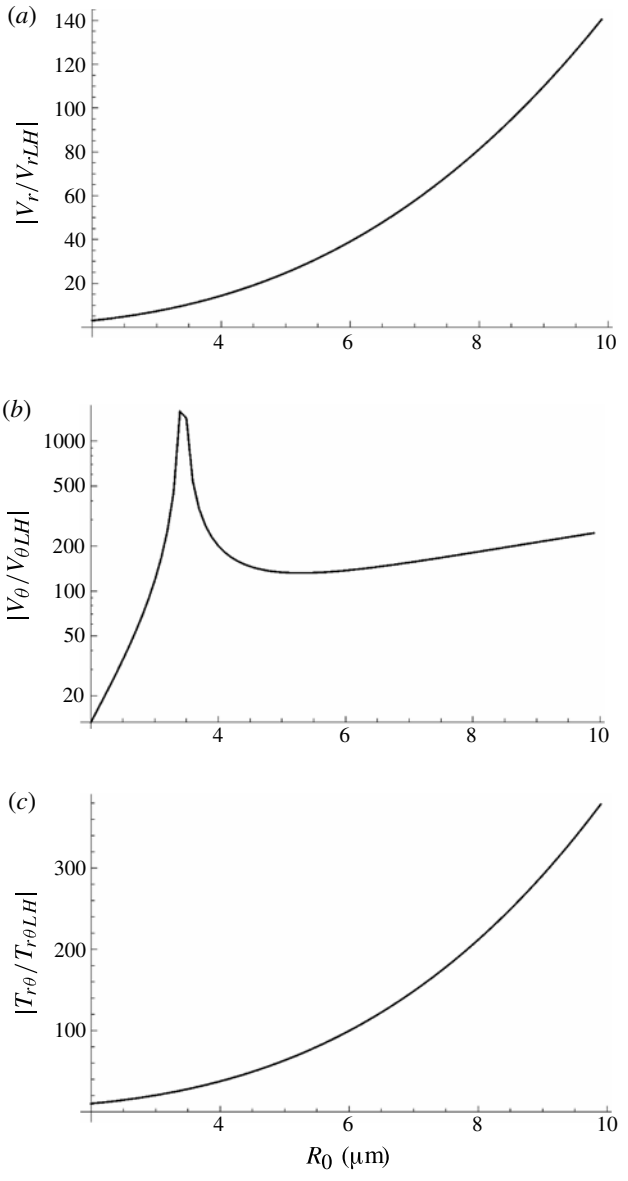


FIGURE 5. Comparison of the streaming characteristics for a bubble in an infinite liquid and in the presence of a wall at different values of R_0. Calculations were made at $d = 5R_0$, $r_1 = R_0 + 2\delta_v$ and $\omega = \omega_{0w}$.

from (2.19) by the use of (2.20) and (2.26), and that in an infinite liquid is found by (4.4). Figure 6(*b*) shows the ratio of the amplitude of the bubble translational velocity in the presence of the wall, $|A\xi_u|$, to that in an infinite liquid, a_T, as a function of the driving frequency for the same values of R_0 and d. The translational velocity amplitude in the presence of the wall is calculated from (2.19) by the use of (2.26) and (2.31), and a_T is calculated from (4.5). As one can see, both the radial oscillation amplitude and the translational velocity amplitude are considerably

https://doi.org/10.1017/jfm.2013.656 Published online by Cambridge University Press

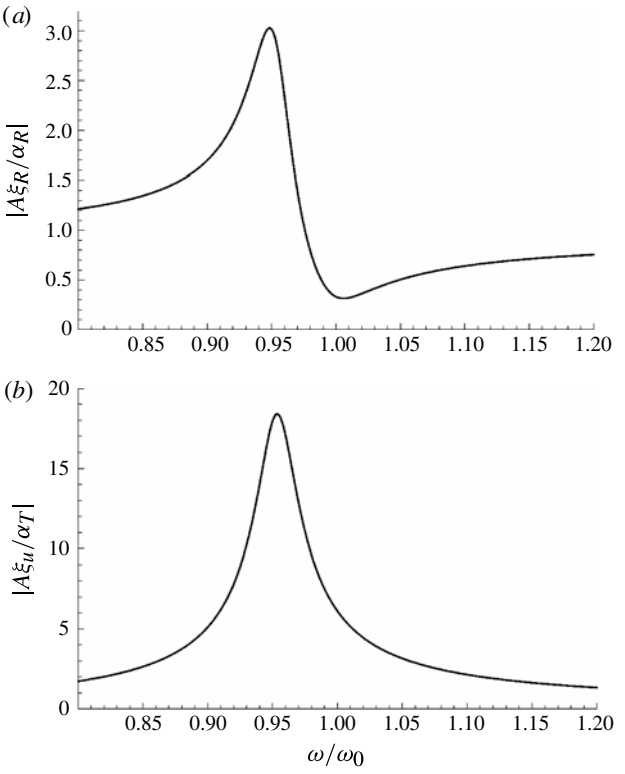


FIGURE 6. (*a*) Ratio of the amplitude of the bubble radial oscillation in the presence of a wall, $|A\xi_R|$, to that in an infinite liquid, a_R, as a function of the driving frequency. (*b*) Ratio of the amplitude of the bubble translational velocity in the presence of a wall, $|A\xi_u|$, to that in an infinite liquid, a_T, as a function of the driving frequency. Calculations were made at $R_0 = 5$ μm and $d = 5R_0$.

higher in the presence of the wall if the bubble is driven at $\omega = \omega_{0w}$. It should be noted, however, that the intensity of microstreaming is also dependent on the phase difference between the radial oscillation and the translational velocity. The leading term in (4.1)–(4.3) is proportional to $\sin\phi$ and hence it has a maximum at $\phi = \pi/2$ and $3\pi/2$ and it vanishes at $\phi = 0$ and π. The dashed curve in figure 7 shows the behaviour of ϕ for a 5 μm radius bubble in an infinite liquid. It was calculated by (4.6). The solid curve in figure 7 shows the behaviour of ϕ for the same bubble in the presence of the wall at $d = 5R_0$. It was obtained using (2.19), (2.20) (2.26) and (2.31). As one can see, in an infinite liquid ϕ is close to π for $\omega = \omega_{0w}$, whereas in the presence of the wall ϕ is close to $\pi/2$, i.e. the value of ϕ in the presence of the wall favours more intense microstreaming. Thus, the presence of the wall changes all three quantities (the radial oscillation amplitude, the translational velocity amplitude and the phase difference between pulsation and translation) in such a way that the intensity of acoustic microstreaming is increased.

Figure 8 illustrates the effect of the Stokes drift velocity. The calculations were made for a bubble with $R_0 = 5$ μm at $r_1 = R_0 + 2\delta_v$ and $d = 5R_0$. The solid lines represent the Eulerian streaming velocity components which are given by (3.19). The dashed lines correspond to the Lagrangian streaming velocity components which are

https://doi.org/10.1017/jfm.2013.656 Published online by Cambridge University Press

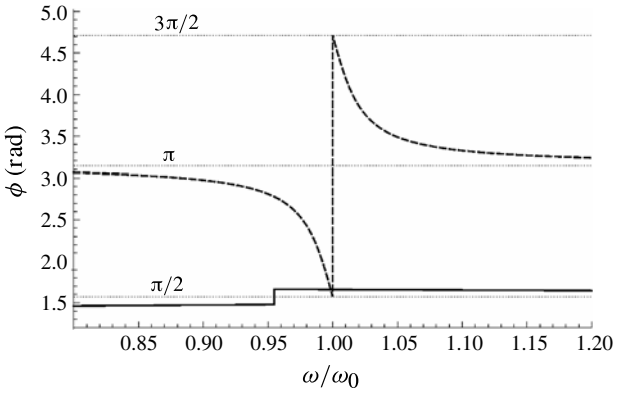


FIGURE 7. Phase difference between the bubble radial oscillation and the bubble translational velocity in an infinite liquid (dashed line) and in the presence of a wall (solid line) as a function of the driving frequency. Calculations were made at $R_0 = 5$ μm and $d = 5R_0$.

calculated from (3.35), (3.38) and (3.39). As one can see, the Stokes drift plays a significant role and leads to a considerable difference between the Eulerian and the Lagrangian tangential velocity components.

For completeness, figure 9 provides an example of acoustic microstreaming that arises in the boundary layer at the wall. The presented results were obtained by (3.45) and (3.46) for a bubble with $R_0 = 2.5$ μm at the driving frequency 1.5 MHz and the acoustic pressure amplitude 50 kPa. Figure 9(*a*) displays the tangential velocity V_τ as a function of the distance τ along the wall surface. The curves demonstrate the behaviour of the velocity at different distances from the wall: $z = d - 0.5\delta_v$, $d - \delta_v$, $d - 2\delta_v$ and $d - 5\delta_v$, where $d = 5R_0$. Figure 9(*b*) shows the tangential stress T_τ exerted on the wall surface at different values of d. As one can see, the intensity of the acoustic microstreaming in the wall boundary layer is much weaker than that around the bubble.

There is one point to be made. Our theory does not impose explicit limitations on the amplitude of the bubble translational velocity and hence on the amplitude of the bubble translational displacement. However, it is generally accepted to assume that the translational displacement should be small compared with the bubble size in order to ignore such effects as the time-averaged drift of the bubble caused by acoustic radiation forces. The bubble translational displacement is proportional to the acoustic pressure amplitude. Therefore the limitation of the translational displacement is in fact a limitation on the acoustic pressure amplitude. The limiting acoustic pressure can be estimated from (2.19) and (2.31). For example, for a bubble with $R_0 = 5$ μm at $d = 5R_0$, the translational displacement does not exceed $0.1R_0$ up to acoustic pressures of 60 kPa, and for a bubble with $R_0 = 2.5$ μm, up to 132 kPa.

5. Conclusion

A theory has been developed that describes acoustic microstreaming around a gas bubble undergoing small radial and translational oscillations in the presence of a distant rigid wall. Equations for acoustic microstreaming in the bulk liquid and in the boundary layer at the wall were obtained. Numerical simulations were performed

https://doi.org/10.1017/jfm.2013.656 Published online by Cambridge University Press

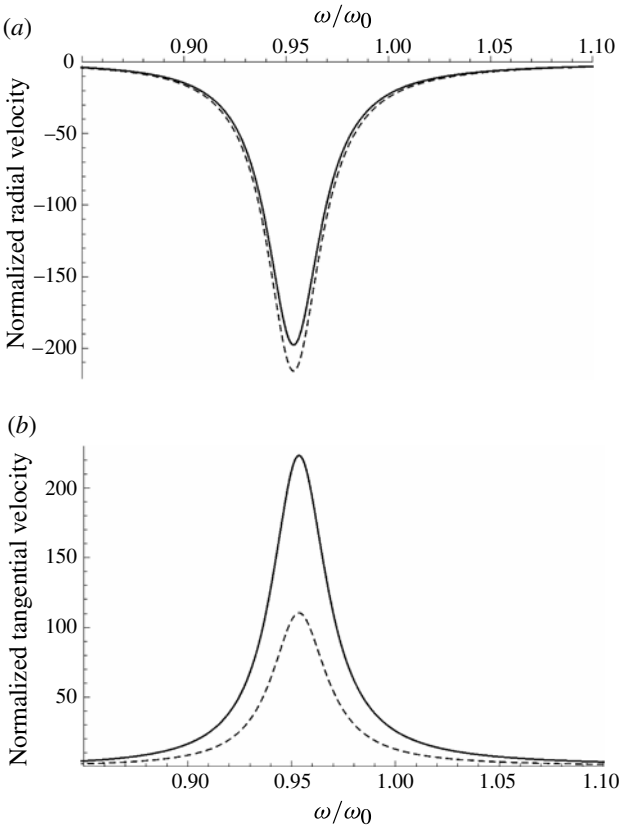


FIGURE 8. Comparison of the Eulerian (solid line) and the Lagrangian (dashed line) streaming velocity components at different values of the driving frequency for a bubble with $R_0 = 5$ μm at $r_1 = R_0 + 2\delta_v$ and $d = 5R_0$.

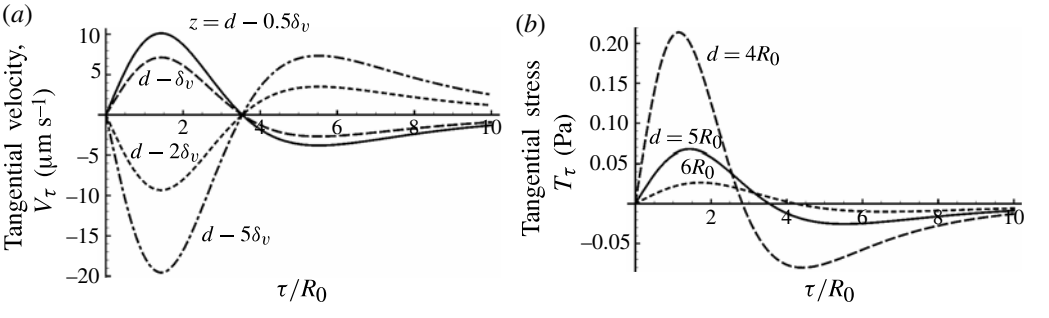


FIGURE 9. Acoustic microstreaming in the boundary layer at the wall. Here τ denotes the distance from the axis z along the wall surface.

to compare acoustic microstreaming generated by a bubble in the presence of a wall to that generated by the same bubble in an infinite liquid. It has been shown that the presence of a wall leads to a considerable increase in the intensity of acoustic

https://doi.org/10.1017/jfm.2013.656 Published online by Cambridge University Press

microstreaming if the bubble is driven at a frequency close to the resonance frequency that the bubble has at the wall. This effect results from the fact that in the presence of the wall the radial oscillation amplitude of the bubble, the amplitude of the bubble translational velocity and the phase difference between the bubble pulsation and translation are changed in a fashion that favours increasing the intensity of acoustic microstreaming.

REFERENCES

ABRAMOWITZ, M. & STEGUN, I. A. 1972 *Handbook of Mathematical Functions*. Dover.

BATCHELOR, G. K. 2000 *An Introduction to Fluid Dynamics*. Cambridge University.

BOYCE, W. E. & DIPRIMA, R. C. 2001 *Elementary Differential Equations and Boundary Value Problems*. 7th edn. Wiley.

COLLIS, J., MANASSEH, R., LIOVIC, P., THO, P., OOI, A., PETKOVIC-DURAN, K. & ZHU, Y. 2010 Cavitation microstreaming and stress fields created by microbubbles. *Ultrasonics* **50**, 273–279.

CRUM, L. A. 1975 Bjerknes forces on bubbles in a stationary sound field. *J. Acoust. Soc. Am.* **57**, 1363–1370.

DAVIDSON, B. J. & RILEY, N. 1971 Cavitation microstreaming. *J. Sound Vib.* **15**, 217–233.

DOINIKOV, A. A. & BOUAKAZ, A. 2010*a* Acoustic microstreaming around a gas bubble. *J. Acoust. Soc. Am.* **127**, 703–709.

DOINIKOV, A. A. & BOUAKAZ, A. 2010*b* Acoustic microstreaming around an encapsulated particle. *J. Acoust. Soc. Am.* **127**, 1218–1227.

ELDER, S. A. 1959 Cavitation microstreaming. *J. Acoust. Soc. Am.* **31**, 54–64.

GOLDBERG, B. B., RAICHLEN, J. S. & FORSBERG, F. 2001 *Ultrasound Contrast Agents: Basic Principles and Clinical Applications*. Martin Dunitz.

KHISMATULLIN, D. B. 2005 Gas microbubbles and their use in medicine. In *Bubble and Particle Dynamics in Acoustic Fields: Modern Trends and Applications* (ed. A. A. Doinikov), pp. 231–289. Research Signpost.

KOLB, J. & NYBORG, W. 1956 Small-scale acoustic streaming in liquids. *J. Acoust. Soc. Am.* **28**, 1237–1242.

LAMB, H. 1975 *Hydrodynamics*. Cambridge University Press.

LANDAU, L. D. & LIFSHITZ, E. M. 1987 *Fluid Mechanics*. Pergamon.

LIU, X. & WU, J. 2009 Acoustic microstreaming around an isolated encapsulated microbubble. *J. Acoust. Soc. Am.* **125**, 1319–1330.

ALONGUET–HIGGINS, M. S. 1998 Viscous streaming from an oscillating spherical bubble. *Proc. R. Soc. Lond.* **454**, 725–742.

MAKSIMOV, A. O. 2007 Viscous streaming from surface waves on the wall of acoustically-driven gas bubbles. *Eur. J. Mech.* B/*Fluids* **26**, 28–42.

MARMOTTANT, P. & HILGENFELDT, S. 2003 Controlled vesicle deformation and lysis by single oscillating bubbles. *Nature* **423**, 153–156.

NYBORG, W. L. 1958 Acoustic streaming near a boundary. *J. Acoust. Soc. Am.* **30**, 329–339.

NYBORG, W. L. 1978 Physical principles of ultrasound. In *Ultrasound: Its Applications in Medicine and Biology* (ed. F. J. Fry), pp. 1–75. Elsevier, Part I.

OGUZ, H. N. & PROSPERETTI, A. 1990 Bubble oscillations in the vicinity of a nearly plane free surface. *J. Acoust. Soc. Am.* **87**, 2085–2092.

PROSPERETTI, A. 1974 Nonlinear oscillations of gas bubbles in liquids: steady-state solutions. *J. Acoust. Soc. Am.* **56**, 878–885.

PROSPERETTI, A. 1977 Thermal effects and damping mechanisms in the forced radial oscillations of gas bubbles in liquids. *J. Acoust. Soc. Am.* **61**, 17–27.

QIN, S., CASKEY, C. F. & FERRARA, K. W. 2009 Ultrasound contrast microbubbles in imaging and therapy: physical principles and engineering. *Phys. Med. Biol.* **54**, R27–R57.

ROONEY, J. A. 1970 Hemolysis near an ultrasonically pulsating gas bubble. *Science* **169**, 869–871.

https://doi.org/10.1017/jfm.2013.656 Published online by Cambridge University Press

ROONEY, J. A. 1972 Shear as a mechanism for sonically induced biological effects. *J. Acoust. Soc. Am.* **52**, 1718–1724.

SCHLICHTING, H. 1979 *Boundary-Layer Theory*. McGraw-Hill.

WU, J. 2002 Theoretical study on shear stress generated by microstreaming surrounding contrast agents attached to living cells. *Ultrasound Med. Biol.* **28**, 125–129.

WU, J. & DU, G. 1997 Streaming generated by a bubble in an ultrasound field. *J. Acoust. Soc. Am.* **101**, 1899–1907.

WU, J. & NYBORG, W. L. 2008 Ultrasound, cavitation bubbles and their interaction with cells. *Adv. Drug. Deliv. Rev.* **60**, 1103–1116.

https://doi.org/10.1017/jfm.2013.656 Published online by Cambridge University Press